



Published in final edited form as:

Ann Biomed Eng. 2013 February ; 41(2): 305–315. doi:10.1007/s10439-012-0651-z.

A Novel Left Heart Simulator for the Multi-modality Characterization of Native Mitral Valve Geometry and Fluid Mechanics

Jean-Pierre Rabbah¹, Neelakantan Saikrishnan, Ph.D.¹, and Ajit P. Yoganathan, Ph.D.¹

¹Wallace H. Coulter Department of Biomedical Engineering, Georgia Institute of Technology and Emory University, Atlanta, GA, USA

Abstract

Numerical models of the mitral valve have been used to elucidate mitral valve function and mechanics. These models have evolved from simple two-dimensional approximations to complex three-dimensional fully coupled fluid structure interaction models. However, to date these models lack direct one-to-one experimental validation. As computational solvers vary considerably, experimental benchmark data are critically important to ensure model accuracy. In this study, a novel left heart simulator was designed specifically for the validation of numerical mitral valve models. Several distinct experimental techniques were collectively performed to resolve mitral valve geometry and hemodynamics. In particular, micro-computed tomography was used to obtain accurate and high-resolution (39 μm voxel) native valvular anatomy, which included the mitral leaflets, chordae tendinae, and papillary muscles. Threedimensional echocardiography was used to obtain systolic leaflet geometry for direct comparison of resultant leaflet kinematics. Stereoscopic digital particle image velocimetry provided all three components of fluid velocity through the mitral valve, resolved every 25 ms in the cardiac cycle. A strong central filling jet was observed during peak systole, with minimal out-of-plane velocities ($V \sim 0.6\text{m/s}$). In addition, physiologic hemodynamic boundary conditions were defined and all data were synchronously acquired through a central trigger. Finally, the simulator is a precisely controlled environment, in which flow conditions and geometry can be systematically prescribed and resultant valvular function and hemodynamics assessed. Thus, these data represent the first comprehensive database of high fidelity experimental data, critical for extensive validation of mitral valve fluid structure interaction simulations.

Keywords

Particle image velocimetry; mitral valve; micro-computed tomography; three-dimensional echocardiography

INTRODUCTION

Disruption of the delicate geometric and mechanical balance between the components of the mitral valve, including the annulus, leaflets, chordae tendineae, and papillary muscles, often results in mitral regurgitation [1–3]. Surgical repair is the preferred medical therapy as it is

Correspondence to: Ajit P. Yoganathan, PhD, Wallace H. Coulter Department of Biomedical Engineering, Georgia Institute of Technology, 313 Ferst Drive, Suite 2119, Atlanta, GA 30332-0535, 404-894-2849, 404-894-4243 (Fax), ajit.yoganathan@bme.gatech.edu.

There were no conflicts of interest to disclose.

considered superior to replacement with reduced operative mortality and thromboembolic complications, while exhibiting greater survival and better preservation of left ventricular function [4,5]. However, surgical repair remains more challenging and the current national repair rate is only 40% [6]. Recent practices to improve pre-operative planning, through the use of real time three-dimensional echocardiography and predictive computational modeling, are expected to help increase repair rates and improve the outcomes [7]. These tools can provide better visualization and understanding of pre-operative mitral valve geometry, lesion indication, and potential post-operative function.

Numerical models of the mitral valve have evolved from simple, two-dimensional mathematical approximations to three-dimensional patient specific models with fluidstructure interaction [8–10]. These evolving methods can provide a unique and noninvasive analysis of mitral valve function and biomechanics, and evaluate fluid flow characteristics pre- and post-operatively [8,11–13]. More recently, medical imaging has been employed to extract patient specific mitral valve anatomy for direct surgical applications, such as patient specific annuloplasty ring design, MitraClip implantation and closure, and predictive virtual modification of the annulus and chordae [13–20].

However, as numerical mitral valve models have grown in complexity, from utilizing patient specific leaflet profiles, inhomogeneous thickness, to prescribed macrostructure, most still lack direct one-to-one experimental validation. Typically, the computed endpoints of the numerical solvers are compared to previously published data, for which only mean values are available, and often result in mismatches in valve geometry and boundary conditions. As computational solvers can vary considerably (from execution with commercially available packages to in-house custom codes), experimental benchmark data are important to ensure model accuracy [21]. Without such validation against benchmark data, the computational model is of “questionable” value in its clinical utility. As rightly pointed out by Einstein and colleagues, “...threedimensional in-vitro flow, deformation and strain data with a native mitral valve are sorely needed.” [22]

Herein, we present a novel left heart simulator designed specifically for the validation of mitral valve fluid structure interaction models. Several distinct experimental techniques were collectively performed to resolve mitral valve geometry and hemodynamics. In particular, micro-computed tomography and three-dimensional echocardiography were used to obtain high-resolution valvular anatomy and systolic leaflet geometry, while stereoscopic digital particle image velocimetry provided detailed characterization of the mitral flow field. In addition, physiologic hemodynamic boundary conditions were defined and all data were synchronously acquired through a central trigger.

MATERIALS AND METHODS

A novel left heart simulator was designed and manufactured for the comprehensive experimental validation of numerical mitral valve models [1–3]. In particular, the modular design was optimized to allow for micro-computed tomography (micro-CT) and digital particle image velocimetry (DPIV) techniques (Figure 1). The valve-mounting chamber was designed such that the same valve could be investigated using multiple experimental methods, without requiring disassembly of the ventricular chamber, or agitation to the mitral valve geometry. The left heart consists of a thin walled acrylic chamber ($t = 0.635$ cm) with a cylindrical cross section ($\Phi = 8.89$ cm), thus making it accessible to micro-CT imaging with quick removal of the aortic and atrial chambers. The cylindrical design results in uniform scattering and x-ray absorption, which results in cleaner valve segmentation. The acrylic thin wall minimizes both x-ray energy absorption and optical refractive index disturbances. The aortic chamber was designed at a 135° angle from the mitral valve to

preserve their physiologic spatial orientation [23]. The aortic chamber houses a 25 mm bi-leaflet mechanical heart valve (Medtronic Parallel; Minneapolis, MN). A cloth covered silicon and acrylic annulus plate allows for mounting native mitral valves. A spring and metal wire drawstring annulus [24] was not used as the metal deleteriously scatters the x-rays creating large image artifacts and poor micro-CT reconstruction. The papillary muscles are attached to papillary muscle holders, which allow for three-dimensional positioning (apical-basal, septal-lateral, anterior-posterior) of the native papillary muscles. The papillary muscles and annulus can be fixed in space for multiple experimental techniques to be performed. The experimental platform closely simulated the physiologic hemodynamic environment of the mitral valve, which was controlled using lumped compliances and resistances. The annulus and papillary muscles holders are also capable of being dynamically adjusted during experimentation to mimic various disease conditions, without requiring any disassembly or stopping the experiment.

Mitral Valve Selection and Preparation

Fresh ovine hearts were procured from a local abattoir. Mitral valves were sized using a Carpentier-Edwards Physio II annuloplasty ring sizer (Edwards Lifesciences; Irving, CA); size 28 mitral valves were selected for this study.

The mitral apparatus – annulus, posterior and anterior leaflets, chordae tendineae, and papillary muscles – were excised from the explanted heart. The mitral annulus was sutured to an annulus plate and the papillary muscles were attached to mechanical rods. The native valve was mounted in the left ventricle of the simulator and the mitral annulus and papillary muscles were set to their normal positions as previously described [25]. The resulting valvular annular geometry and papillary muscle positions were retained throughout each experimental measurement technique. The simulator was filled with 0.9% saline solution and leaflet dynamics and coaptation geometry were studied at room temperature under physiologic hemodynamic conditions (120 mmHg peak left ventricular pressure, 4.8 L/min average cardiac output at a heart rate of 70 beats per minute) to ensure proper valvular function.

Atrial, ventricular, and aortic pressures were measured using pressure transducers (Deltran[®] DPT-200, Utah Medical Products, Inc.; Midvale, UT). An inline electromagnetic flow probe (600 series, Carolina Medical Electronics; East Bend, NC) mounted upstream of the left atrium was used to measure transmitral mitral flow. Data were acquired for 15 cardiac cycles at 1 kHz using a custom LabView Virtual Instrument (v.9.0, 2009, National Instruments Corporation; Austin, TX). A central trigger was used to acquire synchronous data for all modalities.

Three-Dimensional Echocardiography

3D echocardiography images were acquired using a Phillips Intera machine (Phillips iE33 system, Phillips Healthcare; Andover, MA), with an X7-2 pediatric probe. Full volume images were acquired with good temporal resolution (~50 Hz). A validated in-house MATLAB code was used to extract the mitral leaflet geometry for comparison with in-vitro and in-silico leaflet kinematics (Icenogle et al. 2012 in preparation). In short, J-splines were used for semi-automatic segmentation of the posterior and anterior mitral leaflets during peak systole. 18 long axis apical-basal slices across the valve were used for segmentation (slice thickness ~ 2.8 mm) and data were interpolated using an algorithm which was based on the weighted average of the positions of the surrounding points (Butterfly mesh refinement) [26]. This scheme smoothly interpolates new points in any triangular mesh without changing the position of the original vertices. This ensured the user-selected segmentation was not modified during mesh interpolation.

Stereoscopic Digital Particle Image Velocimetry

Following geometry and mechanical characterization of the mitral valve, the *Left Heart Simulator* was adapted for DPIV. The working fluid was 36% glycerin in water, which was used to match the kinematic viscosity of blood (3.5 cSt). The ventricular chamber was immersed in an external rectangular chamber containing the same working fluid to minimize optical distortions resulting from the curved cross-section of the ventricular chamber. Neutrally buoyant fluorescent seeding particles (PMMA with RhB dye, 1–20 μ m, Dantec Dynamics; Denmark) were imaged using a laser light source (Nd:YAG lasers, 17 mJ/pulse, 532 nm, ESI Inc.; Portland, OR). The laser beam was adapted with appropriate optics to create a laser sheet (1 mm thickness) bisecting the mitral valve parallel to the septal-lateral long axis plane (Figure 2). Due to the presence and obstruction of the papillary muscles in the field of view, the angle of the camera was increased ($\sim 30^\circ$) to increase the portion of the flow field that could be imaged. However, the non-orthogonal viewing angle of the camera resulted in velocity bias due to contamination with the out of plane velocity. In order to resolve this bias, as well as to capture the three-dimensional velocity field through the valve, stereoscopic PIV was performed. Two CCD cameras (Imager Pro, 1600 \times 1200 px, LaVision; Germany) with a Nikon Micro-Nikkor 60 mm lens were arranged in a stereoscopic configuration on either side of the ventricular chamber, at an angle to optimize optical access to mitral flow.

The cameras were adapted with Schiempflug adapters to ensure the entire field of view of particles was in focus. An orange filter eliminated reflected laser light (cut-off wavelength = 560nm, Hoya Optics, Santa Clara, CA) and only captured fluorescent scattering from the seeding particles.

To enable stereoscopic reconstruction of the full velocity vector in the plane of interest, a calibration procedure was performed. A three-dimensional two-level target was positioned in the laser sheet plane and imaged from both cameras. Using the Calibration function in DaVis 7.2 (LaVision; Germany), a polynomial mapping function of the image plane was created (Soloff et al 1997). This mapping function was utilized in DaVis 7.2 to reconstruct the three components of velocity in the imaging plane.

Data were acquired at room temperature for adult pulsatile hemodynamic conditions of 4.8 L/min cardiac output, 120 mmHg transmitral pressure at 70 bpm heart rate. 50 phase locked image pairs were acquired every 25 ms in the cardiac cycle. The time difference (dt : 200 to 1000 μ s) between image pairs was optimized for each point in the cardiac cycle to capture high fidelity velocity vectors (particle displacement 5–8 pixels).

Particle cross correlation was performed on the images using multi-pass interrogation with decreasing window size (64 \times 64 to 32 \times 32 pixels) in DaVis 7.2. A single mask was created based on the combined calibrated camera images, such that regions of the imaging plane obstructed from either camera were masked out. Consequently, vectors were only calculated in regions where flow was visible from both cameras, improving data accuracy and minimizing the calculations of erroneous vectors. Since the leaflets of the valve moved during different points in the cardiac cycle, different masks were created for different time points. The resulting vector fields were ensemble averaged and three dimensional velocity fields across the cardiac cycle were obtained.

Micro-computed Tomography

The atrial chamber and aortic section were removed from the left heart simulator, and the left ventricle was fixtured to the micro-CT gantry using a custom adaptor plate. The mitral valve geometry was retained from the earlier hemodynamic characterization. The mitral valve was scanned in air under ambient pressure (~ 1 atm, mitral leaflets were open) using a

vivaCT 40 system (Scanco Medical AG; Brüttisellen, Switzerland). The geometry was acquired at 38 μm voxel size (~600 image slices) using scanning parameters optimized for low density soft tissues (55 keV energy, 109 μA intensity, and 300 ms integration time).

A Gaussian filter ($\sigma = 1.2$, support = 2) was applied to the image data to remove signal noise and improve edge enhancement. Slice by slice user initialized contouring was performed to define the valve anatomy to be included for segmentation. Grey scale images were filtered and converted to binary images using upper and lower bound thresholds. [27] An in-house MATLAB (R2010a, The MathWorks; Natick, MA) program was used to segment mitral valve anatomy through canny edge detection. GeoMagic Studio (12; Morrisville, NC) was used to mesh, smooth, and visualize resultant mitral valve geometry.

RESULTS

Hemodynamic characterization

Representative mitral flow and atrial, ventricular, and aortic pressure are shown in Figure 3. As the flow waveforms were tuned to the same parameters for both saline and glycerin blood analogues, only a single representative waveform is shown (taken from the DPIV experiments). The ensemble averaged mitral flow was 4.8 ± 0.1 L/min, corresponding to a stroke volume of 69.0 ± 2.1 mL; the closing volume was 6.5 ± 0.6 mL. Peak mitral flow rate was 13.2 L/min. Left ventricular pressure peaked at 125.6 ± 1.7 mmHg, and the rate of LVP (dLVP/dt) increase was 1506 ± 52.8 mmHg/sec. Aortic pressure was $122 \pm 1.8/52 \pm 0.9$ mmHg. Diastole lasted approximately 560 msec (as denoted by positive flow through the mitral valve); the remaining 300 msec comprised systole. The mitral valve closed in approximately 100 msec (as observed in the retrograde flow) and remained closed for the remaining 200 msec (zero flow). The results were presented as mean \pm 1 standard deviation.

Geometric characterization

Peak systolic anterior and posterior leaflet geometries segmented from three-dimensional echocardiography are shown in Figure 4. The leaflets demonstrate good closure curvature and functional redundancy creating a competent seal. Annular area was 4.5 cm^2 . Coaptation length at the center of the valve was 5.0 mm; this decreased considerably to 2.0 mm near the commissure. The point of coaptation was 9.3 mm from the anterior annulus and occurred 2.3 mm from the annular plane. Different time points in the cardiac cycle have been similarly segmented for distinct comparison of leaflet motion with numerical simulation across the cardiac cycle.

MicroCT derived geometry is shown in Figure 5. Imaging the valve in air provided excellent contrast for reconstruction. The left ventricular chamber had minimal interference, which allowed a high quality segmentation to be performed. Two defined leaflets with small commissural scallops were observed. Chordae tendineae, derived from each papillary muscle, were inserted into the mitral leaflets. The chordal structures are well defined and show continuous insertions into the free edge, belly, and base of the mitral leaflets. Leaflets and chordal structure are asymmetric and have varying lengths and thicknesses. Comparatively, numerical simulations have begun to apply such geometric features [8,28]. Additionally, unlike present numerical approximations, the chordae do not originate from a singular point on the papillary muscles; chordal insertions vary along the body of each papillary muscle. Chordae also appear to branch or diffuse radially into the mitral leaflet, which is typically not represented numerically. The reconstructed annulus and papillary muscles can be registered to the CAD model of the left heart simulator for use in computational modeling.

Stereoscopic Particle Image Velocimetry (SPIV)

Figure 6 shows the ensemble-averaged vectors fields at four time points in the cardiac cycle. During early systole, the flow field was mostly quiescent when both the mitral and aortic valves were closed (Figure 6a). During early diastole, the mitral valve opens and flow begins to accelerate through the mitral valve. This is indicated by the velocity vectors into the ventricle originating from the mitral orifice. Flow is primarily oriented perpendicular to the mitral annular plane, with some entrainment of fluid from the quiescent portions of the ventricle, particularly near the top and bottom of the image shown here (Figure 6b). The peak velocity of flow through the valve is about 0.4 m/s in the center of the filling jet.

At peak diastole, a strong central filling jet was observed (Figure 6c). The peak velocity observed in this jet was about 0.6 m/s, which is similar to the velocities observed in flow through the mitral valve in clinical studies using echocardiography and in *in vitro* studies on native mitral valves [29–31]. The mitral filling jet appears anteriorly oriented, as indicated by the velocity vectors overlaid on the contour plot. This is indicative of the relative mobility of the two leaflets, with the anterior leaflet having slightly higher mobility resulting in the jet skewing slightly towards the anterior side of the valve. This is similar to jets observed in clinical studies using phase contrast magnetic resonance imaging (PC-MRI) and echo-PIV [32–34]. As suggested by Kilner et al [32], the dominant direction of flow through the mitral valve is observed to be towards the anterior mitral leaflet free edge. This diastolic jet also causes some entrainment of fluid from the quiescent region near the aortic outflow, indicated by the redirection of flow towards the central jet. The Reynolds number of the flow through the mitral valve, based on the cardiac output at peak diastole (15 L/min) and mitral annular area (4.5 cm²) is about 3370.

During end diastole, ventricular pressure increases, slowing and reversing flow through the mitral valve and ultimately forcing it shut. This is indicated by the velocity vectors oriented towards the mitral annulus (Figure 6d). There is minimal flow in the remaining portions of the ventricular chamber during this time point in the cardiac cycle. Since the aortic outflow is out of the field of view during this experiment, the aortic outflow is not seen in this view. No flow was observed when the mitral valve was closed (not shown) as the valve was competent.

Figure 7(A) shows contours of the out-of-plane velocity (W) at peak diastole. The low magnitude of W through the entire field of view indicates that the flow is predominantly two dimensional through the native mitral valve, which can be expected in the central plane of the normal valve. However, it is expected that mitral flow velocity and direction may be affected with abnormal valve geometry, such as with due to leaflet tethering caused by papillary muscle displacement or with edge-to-edge repair. Similar low out-of-plane velocities were observed at all points in the cardiac cycle that were studied. Figure 7(B) shows the out-of-plane vorticity during peak diastolic filling through the mitral valve. As expected, the highest magnitudes of vorticity are observed at the edge of the central filling jet. The region of clockwise fluid rotation, indicated by the negative vorticity values, appears stronger and more coherent compared to the positive vorticity observed near the papillary muscle shown.

DISCUSSION

Surgical strategies and outcomes of mitral valve repairs significantly depend on surgical skill and experience currently [35]. The repair strategy is typically determined based on a 2-D/3-D echocardiographic assessment of the mitral valve and the left ventricle [36,37]. However, in addition to echocardiographic assessment of the valve, it is important to understand and characterize the hemodynamic alterations in the flow through the mitral

valve as a result of disease as well as repair. Numerical models provide the ideal test bed for such a “surgical planning” platform, with their ability to mimic complex repair procedures preoperatively [13–20]. However, high fidelity experimental data are necessary to validate these fluid structure interaction models, before they can be put into widespread clinical use. Unfortunately, the complex geometric and hemodynamic environment associated with the native mitral valve is an extremely challenging platform to obtain high-resolution fluid and geometric data. The current study represents a novel platform to provide these data for one-to-one validation with FSI models.

A novel left heart simulator was designed specifically for the direct experimental validation of computational mitral valve models. Specifically, the modular design allowed multiple experimental techniques to be performed for a single mitral valve without perturbing the geometry. The experimental platform closely simulated the physiologic hemodynamic environment of the mitral valve. The atrial, ventricular, and aortic pressures and the mitral flow were stable and well simulated [38]. Additionally, the waveforms are easily tunable to simulate various pathologies such as hypertension or congestive heart failure.

Geometric characterization was performed using two complementary state of the art medical imaging modalities. Micro-CT imaging was performed because the high spatial resolution was necessary to accurately resolve the detailed and intricate chordal branching. In particular, no other modality is currently capable of reliably imaging the marginal chordae, which control leaflet coaptation, and are thus critical to numerical modeling accuracy. Three-dimensional echocardiography was used because it can non-invasively capture dynamic leaflet motion with sufficient spatial and temporal resolution. Moreover, leaflet geometry can be quantified at any point in the cardiac cycle. Since peak systolic and peak diastolic phases are most often assessed in mitral valve computational models and in clinical diagnosis, these phases are shown in Figure 4. Consequently, the segmented leaflet geometry can be used for direct numerical comparison.

For the first time, stereoscopic digital particle image velocimetry was performed on a native mitral valve with intact subvalvular apparatus to quantify the fluid fields through and proximal to the mitral valve. This well-established technique is capable of measuring velocity vectors with high spatial resolution at any point in the cardiac cycle, which is necessary for the direct quantitative validation of computation fluid dynamics.

The current simulator incorporates many aspects of flow characterization which have not been addressed by previous studies – (1) The full three-dimensional velocity vector was resolved using stereoscopic PIV (2) The entire sub-valvular apparatus was preserved to ensure proper valve opening and closing dynamics (3) The flow through the valve was pulsatile, ensuring the correct dynamic motion of the valve leaflets. Steady flow models can only study one specific time point during the cardiac cycle. (4) Registration of the flow fields to the valve geometry obtained from 3D echo and micro CT is straightforward since all measurements are made on the same valve.

Finally, the simulator presents a precisely tunable environment – bulk hemodynamics and mitral valve geometry can be prescribed. Fluid dynamics proximal and through the mitral valve can be systematically studied under a myriad of carefully tuned conditions. Such studies can provide insight into the relationship between mitral valve geometry and left ventricular filling, and consequently the effects on systolic ejection.

Limitations and Future Studies

While the mechanical and hemodynamic environment of the mitral valve was simulated, some limitations existed. The rigid ventricle used in this study did not mimic native dynamic

annular [39] and ventricular motion. However, previous studies in complimentary experimental and *in vivo* studies have shown that leaflet dynamics compare favorably, in spite of this simplification [40]. Further, the ventricular chamber was not shaped like a native ventricle, hence this study focused only on flow immediately distal to the mitral annulus. However, the relative orientation of the mitral inflow and left ventricular outflow tract was maintained by using an angled aortic section (Figure 1). Only passive mitral filling was simulated in this study. Late diastolic flow as a result of atrial contraction will be simulated in the future using a positive displacement pump upstream of the mitral valve. Different working fluids were used for stereoscopic PIV (36% glycerin) and all other modalities (0.9% saline). Water-glycerin was necessary to (1) minimize optical distortions between the acrylic and fluid, (2) match the kinematic viscosity of blood for more accurate velocity measurements. Since the pressure field across the valve do not change between saline and glycerin, although the Reynolds number is different, the geometry captured in echocardiography should closely match that in the DPIV experiments [41]. This was done because prolonged exposure to glycerin alters valvular material properties. The subvalvular apparatus obstructed portions of the field of view, however this was due to the need for optical access for PIV, which was exacerbated by the need for good viewing windows for two cameras. Future studies could explore the use of echocardiographic PIV to eliminate the need for optical access, however the spatial resolution of that technique might be a limiting factor. The use of non-metallic components could also enable phase contrast magnetic resonance imaging acquisitions on the same valve model.

It should be noted that the work presented in this manuscript represents an $n = 1$. The geometric data presented is that of a singular valve, for which the subsequent experimental conditions were performed. This strategically allows for the direct experimental to computational comparisons. More data on normal, pathological, and repaired mitral valves will be collected as these methods have now been carefully developed and demonstrated. Finally, the valves used in this study (4.5 cm^2) were smaller than previously published ovine studies ($\sim 7 \text{ cm}^2$) [42,43], as limited by the micro-CT field of view; this made direct comparison difficult. However, basic mitral valve geometrical relations were respected when the valve was sutured to the annulus plate and tested. Mainly, the inter-commissural distance was conserved from the explanted heart, while the anterior leaflet comprised two-thirds of the coaptation orifice. Also, the papillary muscles were carefully positioned to result in physiologic coaptation.

In the future, these newly established methods would be combined with the serial acquisition of leaflet strain and chordal forces to characterize mitral valve tissue mechanics [2,3,44,45]. The current work was focused solely on establishing the methods for fluid flow validation, which has previously never been done with a native valve. Additionally, valvular disease, due to abnormal valvular geometry, and subsequent surgical repair will be simulated [1,46]. In particular, mitral regurgitation will be simulated by dilating the mitral annulus and displacing the papillary muscles. Mitral annuloplasty, edge-to-edge repair, and leaflet augmentation techniques could be performed as targeted surgical repairs. Expanded use of echocardiography will provide clinically relevant measures like color Doppler and proximal isovelocity surface area (PISA). Collectively, these studies will improve the surgical planning capabilities of numerical models.

Acknowledgments

This study was funded by a grant from the National Heart Lung and Blood Institute (R01HL092926). The authors would also like to thank Angela Lin for assisting with microCT imaging and reconstruction, JM Machining and Mark McJunkin for manufacturing of flow loop components, and Roy Tweedy's for specimen donation.

REFERENCES

1. He S, Jimenez JH, He Z, Yoganathan AP. Mitral Leaflet Geometry Perturbations with Papillary Muscle Displacement and Annular Dilation: an In-Vitro Study of Ischemic Mitral Regurgitation. *The Journal of Heart Valve Disease*. 2003; 12:300–7. [PubMed: 12803328]
2. Jimenez J, Soerensen DD, He Z, Ritchie J, Yoganathan AP. Effects of Papillary Muscle Position on Chordal Force Distribution: an in-vitro study. *The Journal of Heart Valve Disease*. 2005; 14:295–302. [PubMed: 15974521]
3. Padala M, Hutchison RA, Croft LR, et al. Saddle Shape of the Mitral Annulus Reduces Systolic Strains on the P2 Segment of the Posterior Mitral Leaflet. *The Annals of Thoracic Surgery*. 2009; 88:1499–1504. [PubMed: 19853100]
4. Bonow RO, Carabello BA, Chatterjee K, et al. ACC/AHA 2006 Guidelines for the Management of Patients With Valvular Heart Disease. *Circulation*. 2006; 114:e84–e231. [PubMed: 16880336]
5. Shuhaiber J, Anderson RJ. Meta-analysis of clinical outcomes following surgical mitral valve repair or replacement. *European Journal of Cardio-Thoracic Surgery*. 2007; 31:267–275. [PubMed: 17175161]
6. Adams D, Anyanwu A, Sugeng L, Lang R. Degenerative mitral valve regurgitation: Surgical echocardiography. *Current Cardiology Reports*. 2008; 10:226–232. [PubMed: 18489867]
7. Adams DH, Anyanwu AC. The Cardiologist's Role in Increasing the Rate of Mitral Valve Repair in Degenerative Disease. *Current Opinion in Cardiology*. 2008; 23:105–110. [PubMed: 18303521]
8. Kunzelman KS, Einstein DR, Cochran RP. Fluid–structure interaction models of the mitral valve: function in normal and pathological states. *Philosophical Transactions of the Royal Society B: Biological Sciences*. 2007; 362:1393–1406.
9. Kunzelman KS, Cochran RP, Chuong C, Ring W, Verrier E, Eberhart R. Finite Element Analysis of the Mitral Valve. *The Journal of Heart Valve Disease*. 1993; 2:326–40. [PubMed: 8269128]
10. McQueen DM, Peskin CS, Yellin EL. Fluid dynamics of the mitral valve: physiological aspects of a mathematical model. *American Journal of Physiology - Heart and Circulatory Physiology*. 1982; 242:H1095–H1110.
11. Kunzelman KS, Reimink MS, Cochran RP. Annular dilatation increases stress in the mitral valve and delays coaptation: a finite element computer model. *Cardiovascular Surgery*. 1997; 5:427–434. [PubMed: 9350801]
12. Lau KD, Díaz-Zuccarini V, Scambler P, Burriesci G. Fluid–structure interaction study of the edge-to-edge repair technique on the mitral valve. *Journal of Biomechanics*. 2011; 44:2409–2417. [PubMed: 21767842]
13. Stevanella M, Maffessanti F, Conti C, et al. Mitral Valve Patient-Specific Finite Element Modeling from Cardiac MRI: Application to an Annuloplasty Procedure. *Cardiovascular Engineering and Technology*. 2011; 2:66–76.
14. Pouch AM, Xu C, Yushkevich PA, et al. Semi-automated mitral valve morphometry and computational stress analysis using 3D ultrasound. *Journal of Biomechanics*. 2012; 45:903–907. [PubMed: 22281408]
15. Ionasec RI, Voigt I, Georgescu B, et al. Patient-Specific Modeling and Quantification of the Aortic and Mitral Valves From 4-D Cardiac CT and TEE. *Medical Imaging, IEEE Transactions on*. 2010; 29:1636–1651.
16. Arnoldi, A.; Invernizzi, A.; Ponzini, R.; Votta, E.; Caiani, EG.; Redaelli, A. Mitral Valve Models Reconstructor: a Python based GUI software in a HPC environment for patient-specific FEM structural analysis *Innovations and Advances in Computer Sciences and Engineering*. In: Sobh, T., editor. Netherlands: Springer; 2010. p. 215-219.
17. Hammer, P.; del Nido, P.; Howe, R. Anisotropic Mass-Spring Method Accurately Simulates Mitral Valve Closure from Image-Based Models *Functional Imaging and Modeling of the Heart*. In: Metaxas, D.; Axel, L., editors. Berlin / Heidelberg: Springer; 2011. p. 233-240.
18. Wong VM, Wenk JF, Zhang Z, et al. The Effect of Mitral Annuloplasty Shape in Ischemic Mitral Regurgitation: A Finite Element Simulation. *The Annals of Thoracic Surgery*. 2012; 93:776–782. [PubMed: 22245588]

19. Mansi, T.; Voigt, I.; Mengue, E., et al. Towards Patient-Specific Finite-Element Simulation of MitralClip Procedure Medical Image Computing and Computer-Assisted Intervention. In: Fichtinger, G.; Martel, A.; Peters, T., editors. Berlin / Heidelberg: Springer; 2011. p. 452-459.
20. Tenenholtz, NA.; Hammer, PE.; Schneider, RJ.; Vasilyev, NV.; Howe, RD. IEEE/RSJ International Conference on Intelligent Robots and Systems. San Francisco, California, USA: 2011. On the Design of an Interactive, Patient-Specific Surgical Simulator for Mitral Valve Repair.
21. Stewart S, Paterson E, Burgreen G, et al. Assessment of CFD Performance in Simulations of an Idealized Medical Device: Results of FDA's First Computational Interlaboratory Study. *Cardiovascular Engineering and Technology*. :1–22.
22. Einstein DR, Del Pin F, Jiao X, et al. Fluid–structure interactions of the mitral valve and left heart: Comprehensive strategies, past, present and future. *International Journal for Numerical Methods in Biomedical Engineering*. 2010; 26:348–380.
23. Veronesi F, Corsi C, Sugeng L, et al. A Study of Functional Anatomy of Aortic-Mitral Valve Coupling Using 3D Matrix Transesophageal Echocardiography / CLINICAL PERSPECTIVE. *Circulation: Cardiovascular Imaging*. 2009; 2:24–31. [PubMed: 19808561]
24. Jimenez JH, Liou SW, Padala M, et al. A saddle-shaped annulus reduces systolic strain on the central region of the mitral valve anterior leaflet. *The Journal of thoracic and cardiovascular surgery*. 2007; 134:1562–1568. [PubMed: 18023684]
25. Jimenez JH, Soerensen DD, He Z, He S, Yoganathan AP. Effects of a Saddle Shaped Annulus on Mitral Valve Function and Chordal Force Distribution: An *In-Vitro* Study. *Annals of Biomedical Engineering*. 2003; 31:1171–1181. [PubMed: 14649491]
26. Dyn N, Levin D, Gregory J. Butterfly Subdivision Scheme for Surface Interpolation with Tension Control. *ACM Transactions on Graphics*. 1990; 9:160–9.
27. Bouxsein ML, Boyd SK, Christiansen BA, Guldborg RE, Jepsen KJ, Müller R. Guidelines for assessment of bone microstructure in rodents using micro–computed tomography. *Journal of Bone and Mineral Research*. 2010; 25:1468–1486. [PubMed: 20533309]
28. Votta E, Caiani EG, Veronesi F, Sonicini M, Montevecchi F, Redaelli A. Mitral Valve Finite Element Modelling from Ultrasound Data: Pilot Study for a New Approach to Understand Mitral Function and Clinical Scenarios. *Philos Transact A Math Phys Eng Sci*. 2008; 366:3411–24. [PubMed: 18603525]
29. Kim WY, Walker PG, Pedersen EM, et al. Left ventricular blood flow patterns in normal subjects: A quantitative analysis by three-dimensional magnetic resonance velocity mapping. *Journal of the American College of Cardiology*. 1995; 26:224–238. [PubMed: 7797756]
30. Reul H, Talukder N, Müller EW. Fluid mechanics of the natural mitral valve. *Journal of Biomechanics*. 1981; 14:361–372. [PubMed: 7263728]
31. Domenichini F, Pedrizzetti G, Baccani B. Three-dimensional filling flow into a model left ventricle. *Journal of Fluid Mechanics*. 2005; 539:179–198.
32. Kilner PJ, Yang G-Z, Wilkes AJ, Mohiaddin RH, Firmin DN, Yacoub MH. Asymmetric redirection of flow through the heart. *Nature*. 2000; 404:759–761. [PubMed: 10783888]
33. Kheradvar A, Houle H, Pedrizzetti G, et al. Echocardiographic Particle Image Velocimetry: A Novel Technique for Quantification of Left Ventricular Blood Vorticity Pattern. *Journal of the American Society of Echocardiography*. 2010; 23:86–94. [PubMed: 19836203]
34. Hong G-R, Pedrizzetti G, Tonti G, et al. Characterization and Quantification of Vortex Flow in the Human Left Ventricle by Contrast Echocardiography Using Vector Particle Image Velocimetry. *JACC: Cardiovascular Imaging*. 2008; 1:705–717. [PubMed: 19356506]
35. Bolling SF, Li S, O'Brien SM, Brennan JM, Prager RL, Gammie JS. Predictors of Mitral Valve Repair: Clinical and Surgeon Factors. *The Annals of Thoracic Surgery*. 2010; 90:1904–1912. [PubMed: 21095334]
36. Chikwe J, Adams DH, Su KN, et al. Can three-dimensional echocardiography accurately predict complexity of mitral valve repair? *European Journal of Cardio-Thoracic Surgery*. 2012; 41:518–524. [PubMed: 22223695]

37. Fischer GW, Anyanwu AC, Adams DH. Change in Surgical Management as a Consequence of Real-Time 3D TEE: Assessment of Left Ventricular Function. *Seminars in Cardiothoracic and Vascular Anesthesia*. 2009; 13:238–240. [PubMed: 19951981]
38. Bargiggia G, Bertucci C, Recusani F, et al. A new method for estimating left ventricular dP/dt by continuous wave Doppler-echocardiography. Validation studies at cardiac catheterization. *Circulation*. 1989; 80:1287–1292. [PubMed: 2805264]
39. Rausch M, Bothe W, Kvitting J-P, et al. Characterization of Mitral Valve Annular Dynamics in the Beating Heart. *Annals of Biomedical Engineering*. 2011:1–13.
40. Sacks MS, Enomoto Y, Graybill JR, et al. In-Vivo Dynamic Deformation of the Mitral Valve Anterior Leaflet. *The Annals of Thoracic Surgery*. 2006; 82:1369–1377. [PubMed: 16996935]
41. Yoganathan AP, Corcoran WH, Harrison EC. Pressure drops across prosthetic aortic heart valves under steady and pulsatile flow—In vitro measurements. *Journal of Biomechanics*. 1979; 12:153–164. [PubMed: 422580]
42. Ryan L, Jackson B, Parish L, et al. Quantification and localization of mitral valve tenting in ischemic mitral regurgitation using real-time three-dimensional echocardiography. *European Journal of Cardio-Thoracic Surgery*. 2007; 31:839–844. [PubMed: 17329114]
43. Nguyen TC, Itoh A, Carlhäll CJ, et al. The effect of pure mitral regurgitation on mitral annular geometry and three-dimensional saddle shape. *The Journal of thoracic and cardiovascular surgery*. 2008; 136:557–565. [PubMed: 18805251]
44. Ritchie J, Jimenez J, He Z, Sacks MS, Yoganathan AP. The material properties of the native porcine mitral valve chordae tendineae: An in vitro investigation. *Journal of Biomechanics*. 2006; 39:1129–1135. [PubMed: 16549101]
45. Padala M, Sacks MS, Liou SW, Balachandran K, He Z, Yoganathan AP. Mechanics of the Mitral Valve Strut Chordae Insertion Region. *Journal of Biomechanical Engineering*. 2010; 132:081004. [PubMed: 20670053]
46. Padala M, Powell SN, Croft LR, Thourani VH, Yoganathan AP, Adams DH. Mitral valve hemodynamics after repair of acute posterior leaflet prolapse: Quadrangular resection versus triangular resection versus neochordoplasty. *The Journal of thoracic and cardiovascular surgery*. 2009; 138:309–315. [PubMed: 19619772]

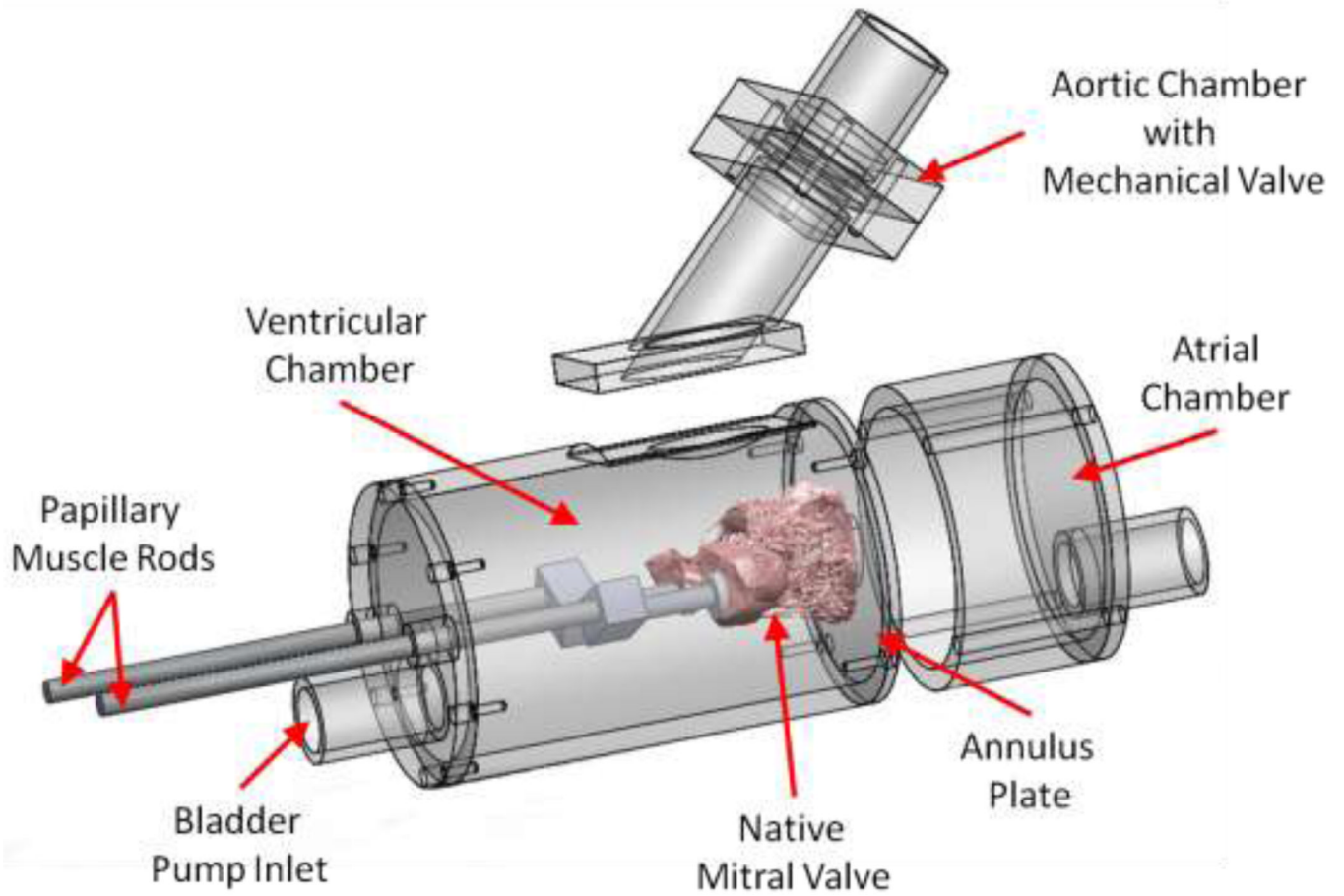


Figure 1. The modular left heart was designed to allow for micro-CT imaging and stereoscopic PIV of native mitral valves. The atrial and aortic chambers are removed, while the left ventricle and mitral valve geometry are left unperturbed.

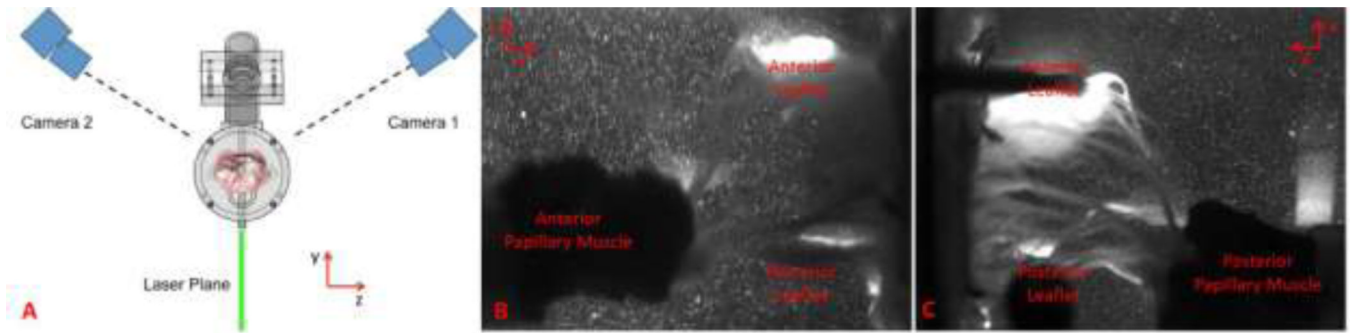


Figure 2. (A) Stereoscopic configuration of the CCD cameras and orientation of the laser plane used for PIV measurements. (B & C) Representative images of the resultant PIV field of view from the two cameras.

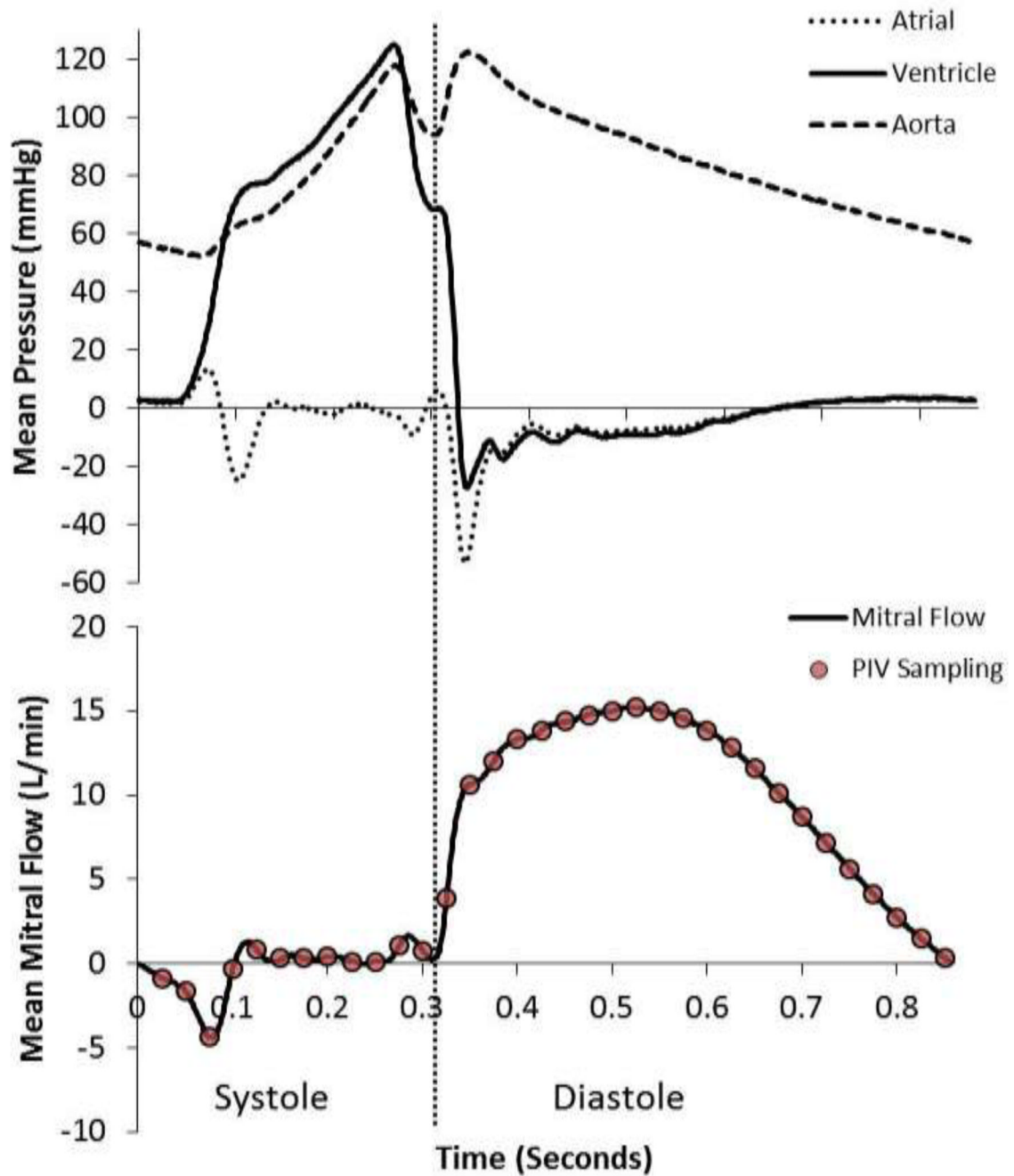


Figure 3.

Atrial (dotted line), ventricular (solid), and aortic pressure (dashed) are plotted for a representative cardiac cycle. Mitral flow is plotted for a representative cardiac cycle. PIV data (red dots) were acquired every 25 ms in the cardiac cycle.

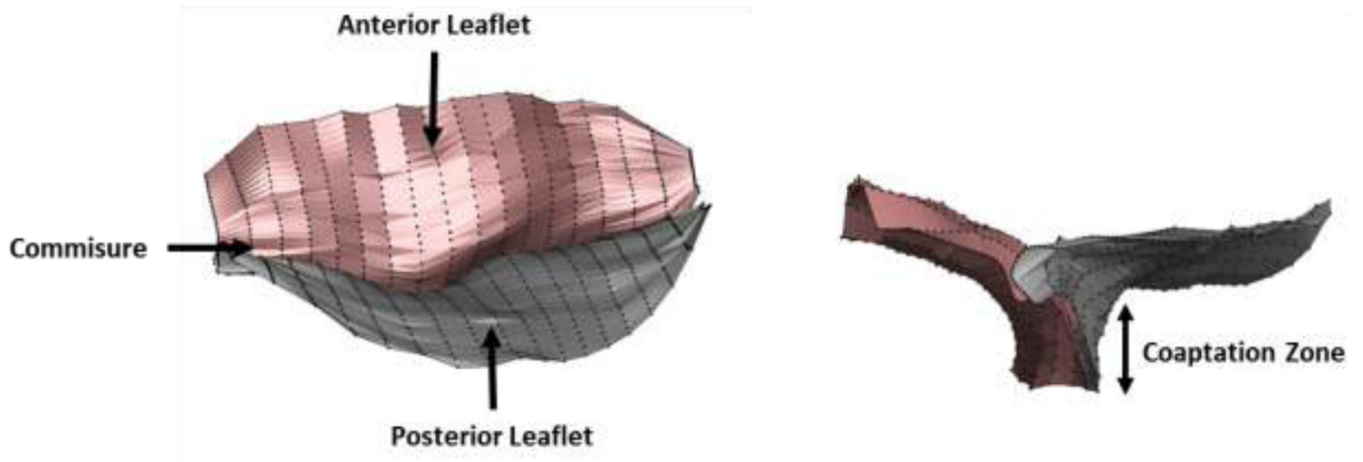


Figure 4. Two views of the segmented mitral leaflets derived from three-dimensional echocardiography are shown. 18 long-axis slices (dotted lines) were used for semi-automated segmentation of the anterior (red) and posterior (grey) leaflets.

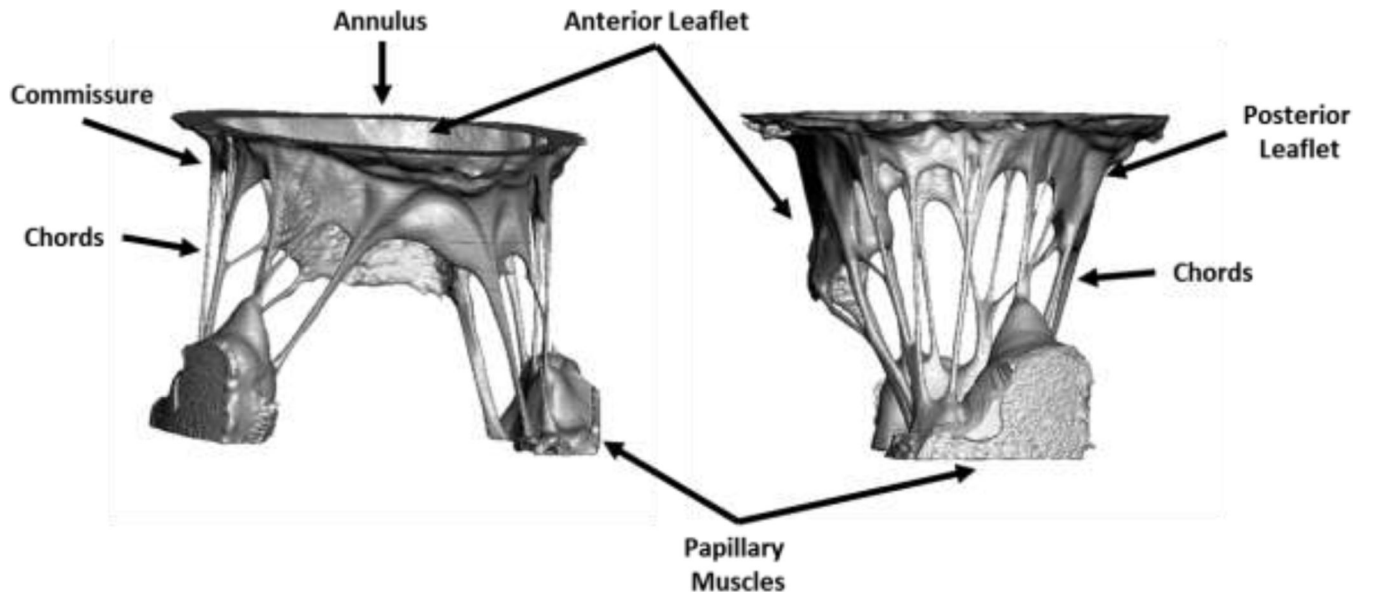


Figure 5. Highly resolved mitral valve geometry as a result of micro-CT imaging and segmentation.

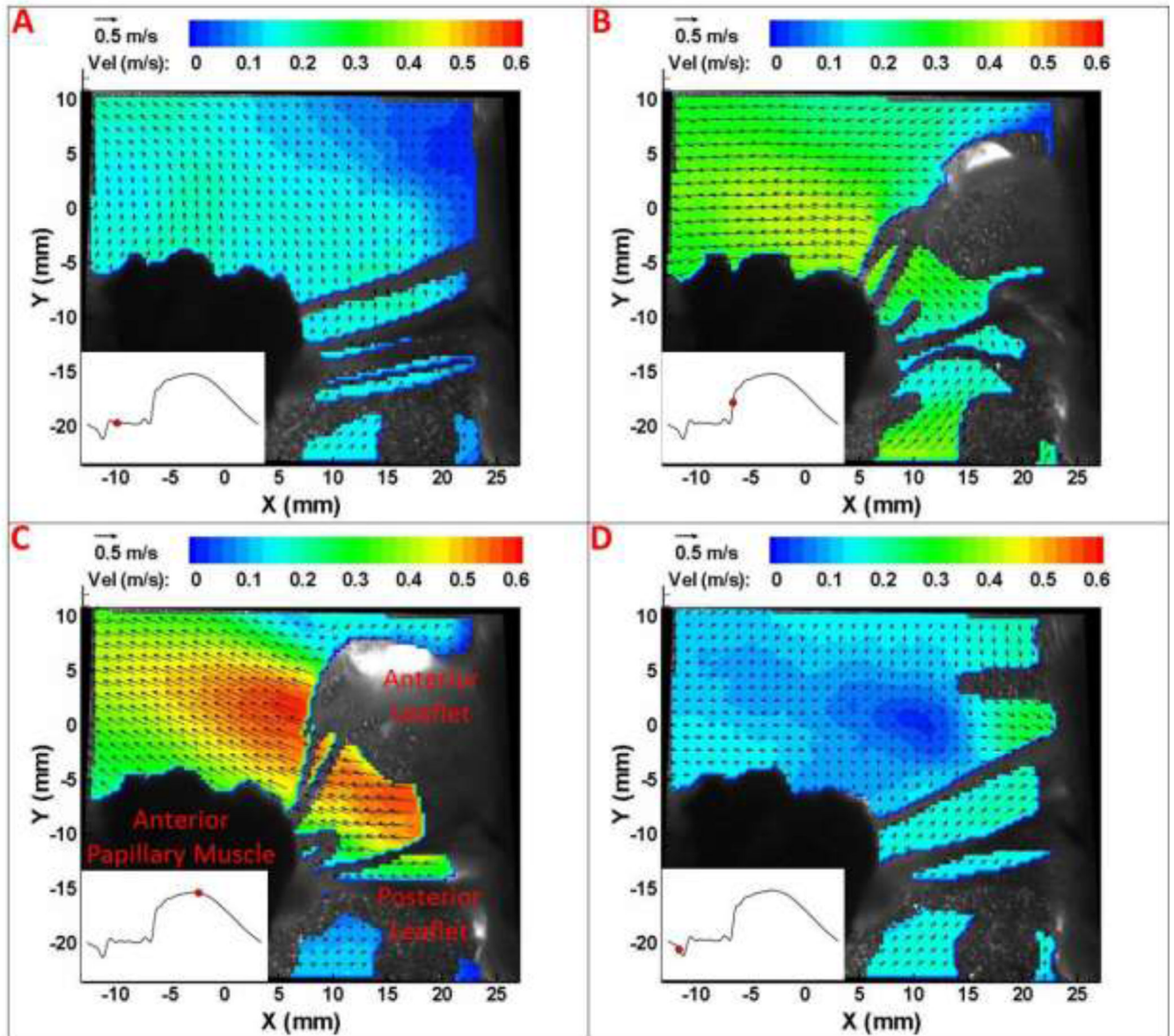


Figure 6. Stereoscopic flow fields through the native mitral valve. Contour plots of the velocity magnitude with superimposed velocity vectors are shown at four points in the cardiac cycle (A) Early systole (B) Early diastole (C) Peak diastole (D) End diastole. The overlaid flow curve is used to indicate the time point in the cardiac cycle where the data were acquired. Image convention for all panels of figure 6 and 7 are shown denoted in panel C.

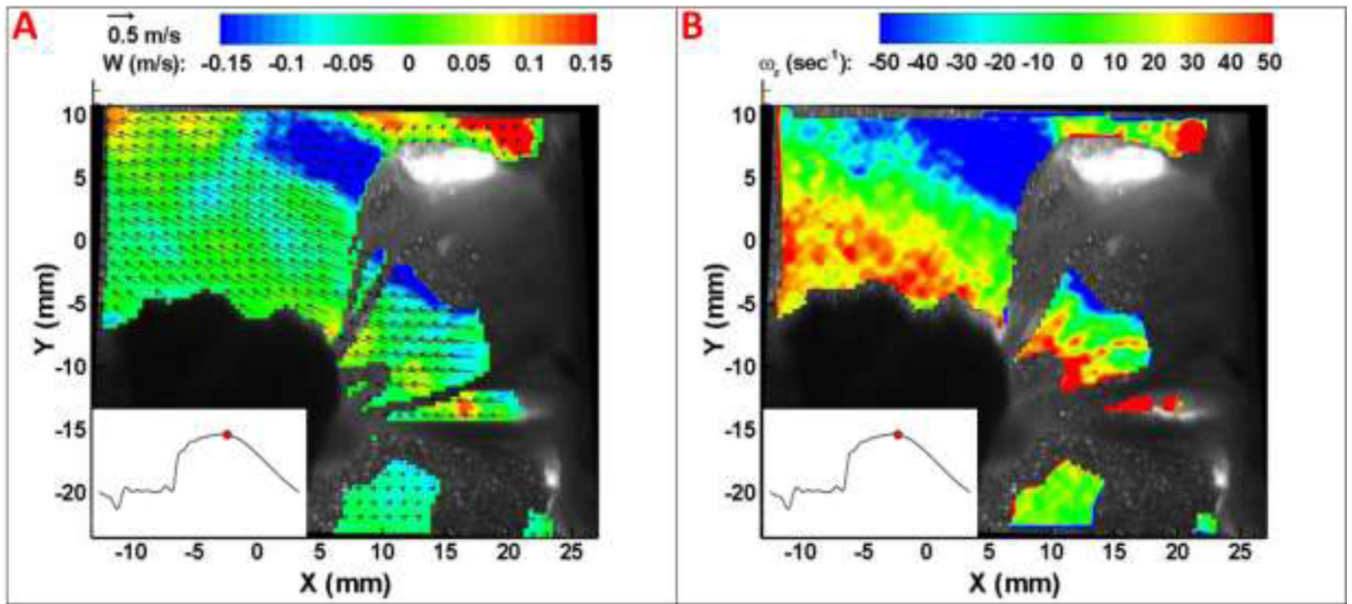


Figure 7.
(A) Contour plot of out-of-plane velocity (W) (B) Contour plot of out-of-plane vorticity.